Measurement of the Cross Section for Prompt Diphoton Production
in $p\overline{p}$ Collisions at $\sqrt{s} = 1.96$ TeV

D. Acosta,[16] J. Adelman,[12] T. Affolder,[9] T. Akimoto,[54] M.G. Albrow,[15] D. Ambrose,[43] S. Amerio,[42] D. Amidei,[33] A. Anastassov,[50] K. Anikeev,[15] A. Annovi,[44] J. Antos,[1] M. Aoki,[54] G. Apollinari,[15] T. Arisawa,[56] J-F. Arguin,[32] A. Artikov,[13] W. Ashmanskas,[15] A. Attal,[7] F. Azfar,[41] P. Azzi-Bacchetta,[42] N. Bacchetta,[42] H. Bachacou,[28] W. Badgett,[15] A. Barbaro-Galtieri,[28] G.J. Barker,[25] V.E. Barnes,[46] B.A. Barnett,[24] S. Baroiant,[6] M. Barone,[17] G. Bauer,[31] F. Bedeschi,[44] S. Behari,[24] S. Belforte,[53] G. Bellettini,[44] J. Bellinger,[58] E. Ben-Haim,[15] D. Benjamin,[14] A. Beretvas,[15] A. Bhatti,[48] M. Binkley,[15] D. Bisello,[42] M. Bishai,[15] R.E. Blair,[2] C. Blocker,[5] K. Bloom,[33] B. Blumenfeld,[24] A. Bocci,[48] A. Bodek,[47] G. Bolla,[46] A. Bolshov,[31] P.S.L. Booth,[29] D. Bortoletto,[46] J. Boudreau,[45] S. Bourov,[15] B. Brau,[9] C. Bromberg,[34] E. Brubaker,[12] J. Budagov,[13] H.S. Budd,[47] K. Burkett,[15] G. Busetto,[42] P. Bussey,[19] K.L. Byrum,[2] S. Cabrera,[14] M. Campanelli,[18] M. Campbell,[33] A. Canepa,[46] M. Casarsa,[53] D. Carlsmith,[58] S. Carron,[14] R. Carosi,[44] M. Cavalli-Sforza,[3] A. Castro,[4] P. Catastini,[44] D. Cauz,[53] A. Cerri,[28] L. Cerrito,[23] J. Chapman,[33] C. Chen,[43] Y.C. Chen,[1] M. Chertok,[6] G. Chiarelli,[44] G. Chlachidze,[13] F. Chlebana,[15] I. Cho,[27] K. Cho,[27] D. Chokheli,[13] J.P. Chou,[20] M.L. Chu,[1] S. Chuang,[58] J.Y. Chung,[38] W-H. Chung,[58] Y.S. Chung,[47] C.I. Ciobanu,[23] M.A. Ciocci,[44] A.G. Clark,[18] D. Clark,[5] M. Coca,[47] A. Connolly,[28] M. Convery,[48] J. Conway,[6] B. Cooper,[30] M. Cordelli,[17] G. Cortiana,[42] J. Cranshaw,[52] J. Cuevas,[10] R. Culbertson,[15] C. Currat,[28] D. Cyr,[58] D. Dagenhart,[5] S. Da Ronco,[42] S. D'Auria,[19] P. de Barbaro,[47] S. De Cecco,[49] G. De Lentdecker,[47] S. Dell'Agnello,[17] M. Dell'Orso,[44] S. Demers,[47] L. Demortier,[48] M. Deninno,[4] D. De Pedis,[49] P.F. Derwent,[15] C. Dionisi,[49] J.R. Dittmann,[15] C. Dörr,[25] P. Doksus,[23] A. Dominguez,[28] S. Donati,[44] M. Donega,[18] J. Donini,[42] M. D'Onofrio,[18] T. Dorigo,[42] V. Drollinger,[36] K. Ebina,[56] N. Eddy,[23] J. Ehlers,[18] R. Ely,[28] R. Erbacher,[6] M. Erdmann,[25] D. Errede,[23] S. Errede,[23] R. Eusebi,[47] H-C. Fang,[28] S. Farrington,[29] I. Fedorko,[44] W.T. Fedorko,[12] R.G. Feild,[59] M. Feindt,[25] J.P. Fernandez,[46] C. Ferretti,[33] R.D. Field,[16] G. Flanagan,[34] B. Flaugher,[15] L.R. Flores-Castillo,[45] A. Foland,[20] S. Forrester,[6] G.W. Foster,[15] M. Franklin,[20] J.C. Freeman,[28] Y. Fujii,[26] I. Furic,[12] A. Gajjar,[29] A. Gallas,[37] J. Galyardt,[11] M. Gallinaro,[48] M. Garcia-Sciveres,[28] A.F. Garfinkel,[46] C. Gay,[59] H. Gerberich,[14] D.W. Gerdes,[33] E. Gerchtein,[11] S. Giagu,[49] P. Giannetti,[44] A. Gibson,[28] K. Gibson,[11] C. Ginsburg,[58] K. Giolo,[46] M. Giordani,[53] M. Giunta,[44] G. Giurgiu,[11] V. Glagolev,[13] D. Glenzinski,[15] M. Gold,[36] N. Goldschmidt,[33] D. Goldstein,[7] J. Goldstein,[41] G. Gomez,[10] G. Gomez-Ceballos,[31] M. Goncharov,[51] O. González,[46] I. Gorelov,[36] A.T. Goshaw,[14] Y. Gotra,[45] K. Goulianos,[48] A. Gresele,[4] M. Griffiths,[29] C. Grosso-Pilcher,[12] U. Grundler,[23] M. Guenther,[46] J. Guimaraes da Costa,[20] C. Haber,[28] K. Hahn,[43] S.R. Hahn,[15] E. Halkiadakis,[47] A. Hamilton,[32] B-Y. Han,[47] R. Handler,[58] F. Happacher,[17] K. Hara,[54] M. Hare,[55] R.F. Harr,[57] R.M. Harris,[15] F. Hartmann,[25] K. Hatakeyama,[48] J. Hauser,[7] C. Hays,[14] H. Hayward,[29] E. Heider,[55] B. Heinemann,[29] J. Heinrich,[43] M. Hennecke,[25] M. Herndon,[24] C. Hill,[9] D. Hirschbuehl,[25] A. Hocker,[47] K.D. Hoffman,[12] A. Holloway,[20] S. Hou,[1] M.A. Houlden,[29] B.T. Huffman,[41] Y. Huang,[14] R.E. Hughes,[38] J. Huston,[34] K. Ikado,[56] J. Incandela,[9] G. Introzzi,[44] M. Iori,[49] Y. Ishizawa,[54] C. Issever,[9] A. Ivanov,[47] Y. Iwata,[22] B. Iyutin,[31] E. James,[15] D. Jang,[50] J. Jarrell,[36] D. Jeans,[49] H. Jensen,[15] E.J. Jeon,[27] M. Jones,[46] K.K. Joo,[27] S.Y. Jun,[11] T. Junk,[23] T. Kamon,[51] J. Kang,[33] M. Karagoz Unel,[37] P.E. Karchin,[57] S. Kartal,[15] Y. Kato,[40] Y. Kemp,[25] R. Kephart,[15] U. Kerzel,[25] V. Khotilovich,[51] B. Kilminster,[38] D.H. Kim,[27] H.S. Kim,[23] J.E. Kim,[27] M.J. Kim,[11] M.S. Kim,[27] S.B. Kim,[27] S.H. Kim,[54] T.H. Kim,[31] Y.K. Kim,[12] B.T. King,[29] M. Kirby,[14] L. Kirsch,[5] S. Klimenko,[16] B. Knuteson,[31] B.R. Ko,[14] H. Kobayashi,[54] P. Koehn,[38] D.J. Kong,[27] K. Kondo,[56] J. Konigsberg,[16] K. Kordas,[32] A. Korn,[31] A. Korytov,[16] K. Kotelnikov,[35] A.V. Kotwal,[14] A. Kovalev,[43] J. Kraus,[23] I. Kravchenko,[31] A. Kreymer,[15] J. Kroll,[43] M. Kruse,[14] V. Krutelyov,[51] S.E. Kuhlmann,[2] S. Kwang,[12] A.T. Laasanen,[46] S. Lai,[32] S. Lami,[48] S. Lammel,[15] J. Lancaster,[14] M. Lancaster,[30] R. Lander,[6] K. Lannon,[38] A. Lath,[50] G. Latino,[36] R. Lauhakangas,[21] I. Lazzizzera,[42] Y. Le,[24] C. Lecci,[25] T. LeCompte,[2] J. Lee,[27] J. Lee,[47] S.W. Lee,[51] R. Lefèvre,[3] N. Leonardo,[31] S. Leone,[44] S. Levy,[12] J.D. Lewis,[15] K. Li,[59] C. Lin,[59] C.S. Lin,[15] M. Lindgren,[15] T.M. Liss,[23] A. Lister,[18] D.O. Litvintsev,[15] T. Liu,[15] Y. Liu,[18] N.S. Lockyer,[43] A. Loginov,[35] M. Loreti,[42] P. Loverre,[49] R-S. Lu,[1] D. Lucchesi,[42] P. Lujan,[28] P. Lukens,[15] G. Lungu,[16] L. Lyons,[41] J. Lys,[28] R. Lysak,[1] D. MacQueen,[32] R. Madrak,[15] K. Maeshima,[15] P. Maksimovic,[24] L. Malferrari,[4] G. Manca,[29] R. Marginean,[38] C. Marino,[23] A. Martin,[24] M. Martin,[59] V. Martin,[37] M. Martínez,[3] T. Maruyama,[54] H. Matsunaga,[54] M. Mattson,[57] P. Mazzanti,[4] K.S. McFarland,[47] D. McGivern,[30] P.M. McIntyre,[51] P. McNamara,[50] R. NcNulty,[29] A. Mehta,[29] S. Menzemer,[31] A. Menzione,[44] P. Merkel,[15] C. Mesropian,[48] A. Messina,[49] T. Miao,[15] N. Miladinovic,[5] L. Miller,[20] R. Miller,[34] J.S. Miller,[33] R. Miquel,[28] S. Miscetti,[17] G. Mitselmakher,[16] A. Miyamoto,[26] Y. Miyazaki,[40] N. Moggi,[4] B. Mohr,[7] R. Moore,[15] M. Morello,[44] P.A. Movilla Fernandez,[28] A. Mukherjee,[15] M. Mulhearn,[31] T. Muller,[25] R. Mumford,[24] A. Munar,[43] P. Murat,[15] J. Nachtman,[15] S. Nahn,[59] I. Nakamura,[43] I. Nakano,[39] A. Napier,[55] R. Napora,[24] D. Naumov,[36] V. Necula,[16] F. Niell,[33] J. Nielsen,[28] C. Nelson,[15] T. Nelson,[15] C. Neu,[43] M.S. Neubauer,[8] C. Newman-Holmes,[15] T. Nigmanov,[45] L. Nodulman,[2] O. Norniella,[3] K. Oesterberg,[21] T. Ogawa,[56]

S.H. Oh,[14] Y.D. Oh,[27] T. Ohsugi,[22] T. Okusawa,[40] R. Oldeman,[49] R. Orava,[21] W. Orejudos,[28] C. Pagliarone,[44] E. Palencia,[10] R. Paoletti,[44] V. Papadimitriou,[15] S. Pashapour,[32] J. Patrick,[15] G. Pauletta,[53] M. Paulini,[11] T. Pauly,[41] C. Paus,[31] D. Pellett,[6] A. Penzo,[53] T.J. Phillips,[14] G. Piacentino,[44] J. Piedra,[10] K.T. Pitts,[23] C. Plager,[7] A. Pompoš,[46] L. Pondrom,[58] G. Pope,[45] X. Portell,[3] O. Poukhov,[13] F. Prakoshyn,[13] T. Pratt,[29] A. Pronko,[16] J. Proudfoot,[2] F. Ptohos,[17] G. Punzi,[44] J. Rademacker,[41] M.A. Rahaman,[45] A. Rakitine,[31] S. Rappoccio,[20] F. Ratnikov,[50] H. Ray,[33] B. Reisert,[15] V. Rekovic,[36] P. Renton,[41] M. Rescigno,[49] F. Rimondi,[4] K. Rinnert,[25] L. Ristori,[44] W.J. Robertson,[14] A. Robson,[41] T. Rodrigo,[10] S. Rolli,[55] L. Rosenson,[31] R. Roser,[15] R. Rossin,[42] C. Rott,[46] J. Russ,[11] V. Rusu,[12] A. Ruiz,[10] D. Ryan,[55] H. Saarikko,[21] S. Sabik,[32] A. Safonov,[6] R. St. Denis,[19] W.K. Sakumoto,[47] G. Salamanna,[49] D. Saltzberg,[7] C. Sanchez,[3] A. Sansoni,[17] L. Santi,[53] S. Sarkar,[49] K. Sato,[54] P. Savard,[32] A. Savoy-Navarro,[15] P. Schlabach,[15] E.E. Schmidt,[15] M.P. Schmidt,[59] M. Schmitt,[37] L. Scodellaro,[10] A. Scribano,[44] F. Scuri,[44] A. Sedov,[46] S. Seidel,[36] Y. Seiya,[40] F. Semeria,[4] L. Sexton-Kennedy,[15] I. Sfiligoi,[17] M.D. Shapiro,[28] T. Shears,[29] P.F. Shepard,[45] D. Sherman,[20] M. Shimojima,[54] M. Shochet,[12] Y. Shon,[58] I. Shreyber,[35] A. Sidoti,[44] J. Siegrist,[28] M. Siket,[1] A. Sill,[52] P. Sinervo,[32] A. Sisakyan,[13] A. Skiba,[25] A.J. Slaughter,[15] K. Sliwa,[55] D. Smirnov,[36] J.R. Smith,[6] F.D. Snider,[15] R. Snihur,[32] A. Soha,[6] S.V. Somalwar,[50] J. Spalding,[15] M. Spezziga,[52] L. Spiegel,[15] F. Spinella,[44] M. Spiropulu,[9] P. Squillacioti,[44] H. Stadie,[25] B. Stelzer,[32] O. Stelzer-Chilton,[32] J. Strologas,[36] D. Stuart,[9] A. Sukhanov,[16] K. Sumorok,[31] H. Sun,[55] T. Suzuki,[54] A. Taffard,[23] R. Tafirout,[32] S.F. Takach,[57] H. Takano,[54] R. Takashima,[22] Y. Takeuchi,[54] K. Takikawa,[54] M. Tanaka,[2] R. Tanaka,[39] N. Tanimoto,[39] S. Tapprogge,[21] M. Tecchio,[33] P.K. Teng,[1] K. Terashi,[48] R.J. Tesarek,[15] S. Tether,[31] J. Thom,[15] A.S. Thompson,[19] E. Thomson,[43] P. Tipton,[47] V. Tiwari,[11] S. Tkaczyk,[15] D. Toback,[51] K. Tollefson,[34] T. Tomura,[54] D. Tonelli,[44] M. Tönnesmann,[34] S. Torre,[44] D. Torretta,[15] S. Tourneur,[15] W. Trischuk,[32] J. Tseng,[41] R. Tsuchiya,[56] S. Tsuno,[39] D. Tsybychev,[16] N. Turini,[44] M. Turner,[29] F. Ukegawa,[54] T. Unverhau,[19] S. Uozumi,[54] D. Usynin,[43] L. Vacavant,[28] A. Vaiciulis,[47] A. Varganov,[33] E. Vataga,[44] S. Vejcik III,[15] G. Velev,[15] V. Veszpremi,[46] G. Veramendi,[23] T. Vickey,[23] R. Vidal,[15] I. Vila,[10] R. Vilar,[10] I. Vollrath,[32] I. Volobouev,[28] M. von der Mey,[7] P. Wagner,[51] R.G. Wagner,[2] R.L. Wagner,[15] W. Wagner,[25] R. Wallny,[7] T. Walter,[25] T. Yamashita,[39] K. Yamamoto,[40] Z. Wan,[50] M.J. Wang,[1] S.M. Wang,[16] A. Warburton,[32] B. Ward,[19] S. Waschke,[19] D. Waters,[30] T. Watts,[50] M. Weber,[28] W.C. Wester III,[15] B. Whitehouse,[55] A.B. Wicklund,[2] E. Wicklund,[15] H.H. Williams,[43] P. Wilson,[15] B.L. Winer,[38] P. Wittich,[43] S. Wolbers,[15] M. Wolter,[55] M. Worcester,[7] S. Worm,[50] T. Wright,[33] X. Wu,[18] F. Würthwein,[8] A. Wyatt,[30] A. Yagil,[15] C. Yang,[59] U.K. Yang,[12] W. Yao,[28] G.P. Yeh,[15] K. Yi,[24] J. Yoh,[15] P. Yoon,[47] K. Yorita,[56] T. Yoshida,[40] I. Yu,[27] S. Yu,[43] Z. Yu,[59] J.C. Yun,[15] L. Zanello,[49] A. Zanetti,[53] I. Zaw,[20] F. Zetti,[44] J. Zhou,[50] A. Zsenei,[18] and S. Zucchelli,[4]

(CDF Collaboration)

[1] *Institute of Physics, Academia Sinica, Taipei, Taiwan 11529, Republic of China*
[2] *Argonne National Laboratory, Argonne, Illinois 60439*
[3] *Institut de Fisica d'Altes Energies, Universitat Autonoma de Barcelona, E-08193, Bellaterra (Barcelona), Spain*
[4] *Istituto Nazionale di Fisica Nucleare, University of Bologna, I-40127 Bologna, Italy*
[5] *Brandeis University, Waltham, Massachusetts 02254*
[6] *University of California at Davis, Davis, California 95616*
[7] *University of California at Los Angeles, Los Angeles, California 90024*
[8] *University of California at San Diego, La Jolla, California 92093*
[9] *University of California at Santa Barbara, Santa Barbara, California 93106*
[10] *Instituto de Fisica de Cantabria, CSIC-University of Cantabria, 39005 Santander, Spain*
[11] *Carnegie Mellon University, Pittsburgh, PA 15213*
[12] *Enrico Fermi Institute, University of Chicago, Chicago, Illinois 60637*
[13] *Joint Institute for Nuclear Research, RU-141980 Dubna, Russia*
[14] *Duke University, Durham, North Carolina 27708*
[15] *Fermi National Accelerator Laboratory, Batavia, Illinois 60510*
[16] *University of Florida, Gainesville, Florida 32611*
[17] *Laboratori Nazionali di Frascati, Istituto Nazionale di Fisica Nucleare, I-00044 Frascati, Italy*
[18] *University of Geneva, CH-1211 Geneva 4, Switzerland*
[19] *Glasgow University, Glasgow G12 8QQ, United Kingdom*
[20] *Harvard University, Cambridge, Massachusetts 02138*
[21] *The Helsinki Group: Helsinki Institute of Physics; and Division of High Energy Physics, Department of Physical Sciences, University of Helsinki, FIN-00044, Helsinki, Finland*
[22] *Hiroshima University, Higashi-Hiroshima 724, Japan*
[23] *University of Illinois, Urbana, Illinois 61801*

24 *The Johns Hopkins University, Baltimore, Maryland 21218*

25 *Institut für Experimentelle Kernphysik, Universität Karlsruhe, 76128 Karlsruhe, Germany*

26 *High Energy Accelerator Research Organization (KEK), Tsukuba, Ibaraki 305, Japan*

27 *Center for High Energy Physics: Kyungpook National University, Taegu 702-701; Seoul National University, Seoul 151-742; and SungKyunKwan University, Suwon 440-746; Korea*

28 *Ernest Orlando Lawrence Berkeley National Laboratory, Berkeley, California 94720*

29 *University of Liverpool, Liverpool L69 7ZE, United Kingdom*

30 *University College London, London WC1E 6BT, United Kingdom*

31 *Massachusetts Institute of Technology, Cambridge, Massachusetts 02139*

32 *Institute of Particle Physics: McGill University, Montréal, Canada H3A 2T8; and University of Toronto, Toronto, Canada M5S 1A7*

33 *University of Michigan, Ann Arbor, Michigan 48109*

34 *Michigan State University, East Lansing, Michigan 48824*

35 *Institution for Theoretical and Experimental Physics, ITEP, Moscow 117259, Russia*

36 *University of New Mexico, Albuquerque, New Mexico 87131*

37 *Northwestern University, Evanston, Illinois 60208*

38 *The Ohio State University, Columbus, Ohio 43210*

39 *Okayama University, Okayama 700-8530, Japan*

40 *Osaka City University, Osaka 588, Japan*

41 *University of Oxford, Oxford OX1 3RH, United Kingdom*

42 *University of Padova, Istituto Nazionale di Fisica Nucleare, Sezione di Padova-Trento, I-35131 Padova, Italy*

43 *University of Pennsylvania, Philadelphia, Pennsylvania 19104*

44 *Istituto Nazionale di Fisica Nucleare, University and Scuola Normale Superiore of Pisa, I-56100 Pisa, Italy*

45 *University of Pittsburgh, Pittsburgh, Pennsylvania 15260*

46 *Purdue University, West Lafayette, Indiana 47907*

47 *University of Rochester, Rochester, New York 14627*

48 *The Rockefeller University, New York, New York 10021*

49 *Istituto Nazionale di Fisica Nucleare, Sezione di Roma 1, University di Roma "La Sapienza," I-00185 Roma, Italy*

50 *Rutgers University, Piscataway, New Jersey 08855*

51 *Texas A&M University, College Station, Texas 77843*

52 *Texas Tech University, Lubbock, Texas 79409*

53 *Istituto Nazionale di Fisica Nucleare, University of Trieste/ Udine, Italy*

54 *University of Tsukuba, Tsukuba, Ibaraki 305, Japan*

55 *Tufts University, Medford, Massachusetts 02155*

56 *Waseda University, Tokyo 169, Japan*

57 *Wayne State University, Detroit, Michigan 48201*

58 *University of Wisconsin, Madison, Wisconsin 53706*

59 *Yale University, New Haven, Connecticut 06520*

(Dated: February 4, 2008)

We report a measurement of the rate of prompt diphoton production in $p\overline{p}$ collisions at $\sqrt{s} = 1.96$ TeV using a data sample of 207 pb^{-1} collected with the upgraded Collider Detector at Fermilab (CDF II). The background from non-prompt sources is determined using a statistical method based on differences in the electromagnetic showers. The cross section is measured as a function of the diphoton mass, the transverse momentum of the diphoton system, and the azimuthal angle between the two photons and is found to be consistent with perturbative QCD predictions.

PACS numbers: 13.83.Qk, 12.38.Qk

Diphoton ($\gamma\gamma$) final states are a signature of many interesting physics processes. For example, at the LHC, one of the main discovery channels for the Higgs search is the $\gamma\gamma$ final state [1, 2]. An excess of $\gamma\gamma$ production at high invariant mass could be a signature of large extra dimensions [3], and in many theories involving physics beyond the standard model, cascade decays of heavy new particles generate a $\gamma\gamma$ signature [4]. However, the QCD production rate is large compared to most new physics, so an understanding of the QCD production mechanism is a prerequisite to searching reliably for new physics in this channel. In addition, the two-photon final state is interesting in its own right. Due to the excellent energy resolution of the CDF electromagnetic (EM) calorimeter, the 4-momenta of the two photons in the final state can be determined with good precision. This allows, for

example, a direct measurement of the transverse momentum of the $\gamma\gamma$ system (q_T), which is sensitive to initial state soft gluon radiation.

In perturbative Quantum Chromodynamics (pQCD), the leading contributions are from quark anti-quark annihilation ($q\bar{q} \to \gamma\gamma$) and gluon-gluon scattering ($gg \to \gamma\gamma$). The latter subprocess involves initial state gluons coupling to the final state photons through a quark box; thus, this subprocess is suppressed by a factor of α_s^2 with respect to the $q\bar{q}$ subprocess. However, the rate is still appreciable in kinematic regions where the gg parton luminosity is high, such as at low $\gamma\gamma$ mass. Because the probability for a hard parton to fragment to a photon is of order α_{em}/α_s, processes involving the production of one (zero) prompt photons and one (two) photons originating from parton fragmentation are also effectively of leading order (LO). Next-to-leading order (NLO) contributions include real and virtual corrections to the above subprocesses.

We have compared our experimental results to three predictions : DIPHOX [5], ResBos [6], and PYTHIA [7]. DIPHOX is a fixed-order QCD calculation that includes all of the above subprocesses at NLO (except for $gg \to \gamma\gamma$ which is present only at LO). Recently, NLO corrections for $gg \to \gamma\gamma$ have been calculated [8] and we have added these corrections to the DIPHOX prediction. The ResBos program includes subprocesses where the two photons are produced at the hard-scattering at NLO and fragmentation contributions at LO; but also resums the effects of initial state soft gluon radiation. This is particularly important for examination of the $\gamma\gamma$ q_T distribution, which is a delta function at LO and divergent as $q_T \to 0$ at NLO, and thus requires a soft gluon resummation in order to provide a physical description of the $\gamma\gamma$ data in this region. PYTHIA is a parton shower Monte Carlo program that contains the above processes at LO.

At hadron-hadron colliders, it is difficult to measure a fully inclusive $\gamma\gamma$ cross section due to the large backgrounds from quarks and gluons fragmenting into neutral mesons which carry most of the parent parton's momentum. Isolation requirements are typically used to reduce these backgrounds. In this analysis, the isolation criterion requires that the transverse energy (E_T) sum in a cone of radius $R = 0.4$(in $\eta - \phi$ space) [9] about the photon direction, minus the photon energy, be less than 1 GeV. This isolation requirement reduces the backgrounds from neutral mesons decaying into photons and photon production from fragmentation sources. The CDF isolation requirement effectively removes all contributions where both photons originate from fragmentation subprocesses. However, as will be noted later, some indication of single fragmentation subprocesses can still be observed in the CDF data.

The CDF II detector is a magnetic spectrometer which is described in detail elsewhere [10]. The central detector consists of a silicon micro-strip vertex detector in-

side a cylindrical drift chamber, both of which are immersed in the 1.4 T magnetic field of a superconducting solenoid. Outside the solenoid is the central calorimeter which is divided into an electromagnetic compartment (CEM) on the inside and hadronic compartment (CHA) on the outside. Both calorimeters are segmented into towers of granularity $\Delta\eta \times \Delta\phi \approx 0.1 \times 0.26$. The CEM consists of a scintillator-lead calorimeter along with an embedded multi-wire proportional chamber (CES) located near shower maximum at 6 radiation lengths. The CES allows for a position determination of the EM shower and for a measurement of the lateral shower profile. The average energy resolution of the CEM is $\sigma(E)/E = 13.5\%/\sqrt{E\sin\theta}$ (with E in GeV) and the position resolution of the CES is 2 mm for a 50 GeV photon. Another important component for this analysis is a preshower wire chamber (CPR) mounted between the magnet coil and the CEM, at about $1.2/\sin\theta$ radiation lengths. The CPR detects photon candidates that have converted in the magnet coil and other material in the inner detector.

This analysis [11] uses events collected with a trigger that requires two photon candidates with E_T greater than 12 GeV each. A requirement of E_T greater than 14 GeV (13 GeV) for the leading (softer) photon candidate in the event is imposed in the offline analysis. The minimum transverse energy requirements for the two photon candidates are different in order to avoid the kinematic region where the NLO calculation is unstable due to the imperfect cancellation of the real and virtual gluon divergences.

In identifying photons, we impose fiducial requirements to avoid uninstrumented regions at the edges of the CES; as part of this criterion we require the pseudorapidity of the photon candidate to be in the interval $|\eta| < 0.9$. The reconstructed z-vertex for the collision is required to be less than 60 cm from the center of the detector. The ratio of the hadronic energy to EM energy (Had/EM) for the photon candidates must be less than $0.055+0.00045\times E$, with E the EM energy in GeV. The isolation energy is required to be below 1 GeV. Although only about 1% of showers from prompt photons have more than 1 GeV of additional energy in the isolation cone, about 15% of the photon showers fail the isolation requirement because of additional energy from the underlying event [12]. Photon candidates with any tracks (p_T above 0.5 GeV) that can be extrapolated to them are rejected. The lateral profile of EM showers in the CES is compared to the profile of electrons measured in a test beam. The definition of the χ^2 from the comparison can be found in Ref. [13]. We require the χ^2 of the comparison to be less than 20 in the event selection and reject photon candidates with an additional CES cluster above 1 GeV [14]. The efficiencies for each event selection requirement, evaluated using a combination of PYTHIA Monte Carlo and data, are listed sequentially in Table I.

TABLE I: The selection efficiencies per diphoton event.

Trigger efficiency	0.951
Reconstruction efficiency and fiducial	0.423
Isolation energy in 0.4 cone < 1 GeV	0.727
No track pointing to the EM cluster	0.699
No extra CES cluster above 1 GeV	0.899
CES $\chi^2 < 20$	0.970
Had/EM $<0.055 + 0.00045 \times E$	0.976
|z-vertex | < 60 cm	0.877
Combined (ε_{tot})	0.152

TABLE II: A comparison of the cross section as a function of the $\gamma\gamma$ mass for the data and predictions from DIPHOX, ResBos and PYTHIA.

$M_{\gamma\gamma}$ (GeV)	CDF Data (pb/GeV)	DIPHOX (pb/GeV)	ResBos (pb/GeV)	PYTHIA (pb/GeV)
10-25	$0.03 \pm 0.03 \pm 0.01$	0.04	0.01	0.01
25-30	$0.44 \pm 0.13 \pm 0.12$	0.41	0.31	0.18
30-35	$0.61 \pm 0.17 \pm 0.16$	0.70	0.65	0.38
35-45	$0.46 \pm 0.10 \pm 0.14$	0.46	0.43	0.24
45-60	$0.16 \pm 0.05 \pm 0.04$	0.19	0.16	0.09
60-100	$0.01 \pm 0.02 \pm 0.01$	0.04	0.04	0.02

TABLE III: A comparison of the cross section as a function of the $\gamma\gamma$ q_T for the data and predictions from DIPHOX, ResBos and PYTHIA.

q_T (GeV)	CDF Data (pb/GeV)	DIPHOX (pb/GeV)	ResBos (pb/GeV)	PYTHIA (pb/GeV)
0-1	$0.70 \pm 0.30 \pm 0.14$	-2.45	0.34	0.53
1-2	$1.18 \pm 0.43 \pm 0.28$	5.59	0.95	1.15
2-4	$0.92 \pm 0.35 \pm 0.28$	2.06	1.03	0.94
4-8	$0.96 \pm 0.23 \pm 0.32$	1.17	0.94	0.46
8-12	$0.29 \pm 0.21 \pm 0.13$	0.44	0.59	0.21
12-16	$0.42 \pm 0.14 \pm 0.12$	0.24	0.36	0.12
16-24	$0.19 \pm 0.09 \pm 0.05$	0.13	0.19	0.07
24-32	$0.12 \pm 0.06 \pm 0.03$	0.09	0.07	0.03
32-40	$0.10 \pm 0.05 \pm 0.05$	0.06	0.03	0.01

The trigger efficiency per photon, measured using a single photon trigger, is approximately 80% at 13 GeV and rises to greater than 99% for photons above 15 GeV. The combined selection efficiency (ε_{tot}), including acceptance and trigger efficiency, is 15.2% per diphoton event.

After imposing all of the requirements, 889 two-photon candidates remain in our data sample. This sample includes background from neutral mesons such as π^0 and η that decay to multiple photons. To estimate this background, we apply the statistical background subtraction method described in [15], which makes use of the differences on average between EM showers produced by single photons and by the multiple photons produced in neutral meson decays. The separation between single and multiple photon showers relies on the shower shape measured by the CES χ^2 and the preshower conversion pulse height measured by the CPR. Since photons from the decay of neutral mesons with E_T above 35 GeV are almost collinear in the lab frame, their shower shape in the CES is no longer distinguishable from a single-photon shower. To estimate the background contamination in this high E_T region, the CPR has been utilized. The chance for a conversion to take place in the tracking volume or magnet coil (1.1 radiation lengths) and generating a hit in the CPR is higher for the multiple photons than for a single photon. We use the CES shower shape for photon showers with $E_T < 35$ GeV and the CPR pulse height for $E_T > 35$ GeV. For each photon candidate, we test whether the CES χ^2 is less than 4 (low E_T) or the photon canidate produces a pulse height in the CPR greater than one minimum ionizing particle (high E_T). There are four possibilities for the final state: both candidates pass the test, the first candidate passes and the second fails, the first fails and the second passes, or both candidates fail (the first candidate has the higher E_T). From the known efficiencies for photons and background to pass the χ^2 and conversion tests, we can then determine the number of true $\gamma\gamma$ events (as well as the number of γ-background, background-γ and background-background events). Using the two background techniques discussed, we determine that of the 889 candidates, $427 \pm 59(stat)$ are real $\gamma\gamma$ events. From these events, the calculated ac-

ceptance and the integrated luminosity, we determine the diphoton cross sections for several kinematic variables. The $\gamma\gamma$ mass distribution is shown in Fig. 1, along with predictions from DIPHOX, ResBos and PYTHIA. The q_T distribution is shown in Fig. 2, and the $\Delta\phi$ distribution between the two photons is shown in Fig. 3. The vertical error bars on the data indicate the combined statistical and systematic uncertainties with the inner tick marks indicating the statistical uncertainty alone [16]. The PYTHIA predictions have been scaled (factor of 2) to the total measured cross section in all the figures. The cross sections as a function of these three different variables are also tabulated in Tables II, III and IV.

It should be noted that the background to the $\gamma\gamma$ signal has been determined independently for each kinematic bin as the background fraction can vary with the kinematics. Determining the background on a bin-by-bin basis increases the statistical uncertainty but decreases the systematic uncertainty.

The systematic effects include uncertainties on the selection efficiencies (11%), uncertainties from the background subtraction (20-30%) and from the luminosity determination (6%) [17].

We note some features of the theoretical predictions. The gg subprocess provides a significant contribution to diphoton production at low mass ($\sim$30 GeV/c^2); the slight wiggle observed in the DIPHOX prediction is due to the very rapid falloff (with diphoton mass) of the gg subprocess compared to the $q\bar{q}$ subprocess. The Res-

TABLE IV: A comparison of the cross section as a function of the $\gamma\gamma$ $\Delta\phi$ for the data and predictions from DIPHOX, ResBos and PYTHIA.

$\Delta\phi_{\gamma\gamma}$ (π rad)	CDF Data (pb/rad)	DIPHOX (pb/rad)	ResBos (pb/rad)	PYTHIA (pb/rad)
0.0-0.2	$1.06 \pm 0.52 \pm 0.34$	0.69	0.01	0.02
0.2-0.4	$0.89 \pm 0.52 \pm 0.32$	0.56	0.23	0.09
0.4-0.6	$0.51 \pm 0.63 \pm 0.19$	0.71	0.73	0.44
0.6-0.8	$3.34 \pm 1.10 \pm 1.04$	1.83	3.08	1.09
0.8-1.0	$15.56 \pm 2.59 \pm 4.70$	23.37	17.52	10.68

Bos q_T curve is smooth for the entire range, while the DIPHOX curve (as can be seen by the negative value in the first bin of Table III) is unstable at low q_T due to the singularity noted earlier, and thus is not plotted in Fig. 2 for $q_T < 2$ GeV/c [18]. At the high q_T end, DIPHOX displays a shoulder, a feature absent in the ResBos prediction. The ResBos curve lies above the DIPHOX one at $\Delta\phi$ values of the order of $\pi/2$ but also lies significantly below the DIPHOX curve at small $\Delta\phi$.

The observed differences between the predictions are expected. The fragmentation contribution in ResBos is effectively at LO. Since fragmentation to a photon is of order α_{em}/α_s, some 2→3 processes such as $qg \rightarrow gq\gamma$, where the quark in the final state fragments to a second photon, are of order $\alpha_{em}^2\alpha_s$ and are included in a full NLO calculation. These contributions are present in DIPHOX, but not in ResBos, which leads to an underestimate of the production rate in the latter at high q_T, low $\Delta\phi$, and low $\gamma\gamma$ mass. In particular, the shoulder at q_T of approximately 30 GeV/c arises from an increase in phase space for both the direct and fragmentation subprocesses [19]. It is instructive to divide the DIPHOX predictions into two regions : $\Delta\phi > \pi/2$ and $\Delta\phi < \pi/2$. We do so, and plot the q_T prediction for the $\Delta\phi < \pi/2$ region in Fig. 2 in order to highlight this contribution. It is apparent that the bump in the DIPHOX prediction at a q_T of approximately 30 GeV/c is due to the "turn-on" of the $\Delta\phi < \pi/2$ region of phase space. At $\Delta\phi$ values above $\pi/2$, the effects from soft gluon emission (included in ResBos but not in DIPHOX) are significant.

The data are in good agreement with the predictions for the mass distribution. At low to moderate q_T and $\Delta\phi$ greater than $\pi/2$, where the effect of soft gluon emissions are important, the data agree better with ResBos than DIPHOX. By contrast, in the regions where the 2→3 fragmentation contribution becomes important, large q_T, $\Delta\phi$ less than $\pi/2$ and low diphoton mass, the data agree better with DIPHOX.

In this paper, we have presented results for $\gamma\gamma$ production in $p\bar{p}$ collisions at a center-of-mass energy of 1.96 TeV using a data sample twice that previously available. Good agreement has been observed with resummed and NLO predictions in different regions of phase space. For agreement in all areas, however, a resummed full NLO
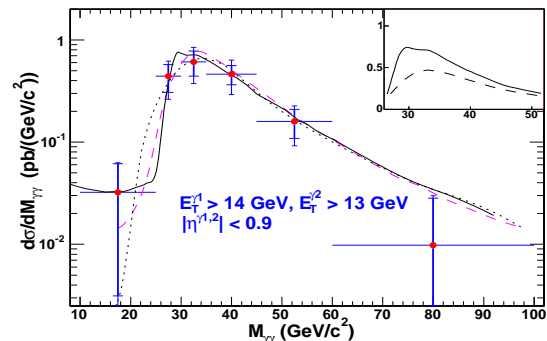

FIG. 1: The $\gamma\gamma$ mass distribution from the CDF Run II data, along with predictions from DIPHOX (solid), ResBos (dashed), and PYTHIA (dotted). The PYTHIA predictions have been scaled by a factor of 2. The inset shows, on a linear scale, the total $\gamma\gamma$ cross section in DIPHOX with (solid)/without (dashed) the gg contribution.
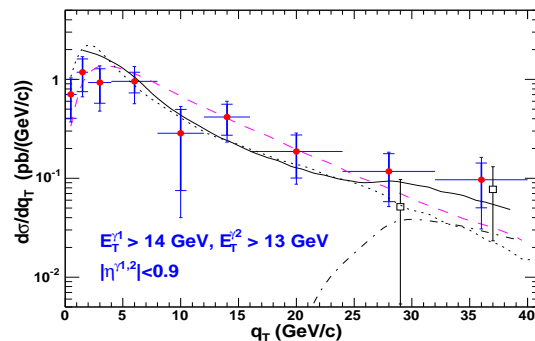

FIG. 2: The $\gamma\gamma$ q_T distribution from the CDF Run II data, along with predictions from DIPHOX (solid), ResBos (dashed), and PYTHIA (dotted). The PYTHIA predictions have been scaled by a factor of 2. Also shown, at larger q_T, are the DIPHOX prediction (dot-dashed) and the CDF Run II data (open squares : shifted to the right by 1 GeV for visibility) for the configuration where the two photons are required to have $\Delta\phi < \pi/2$.

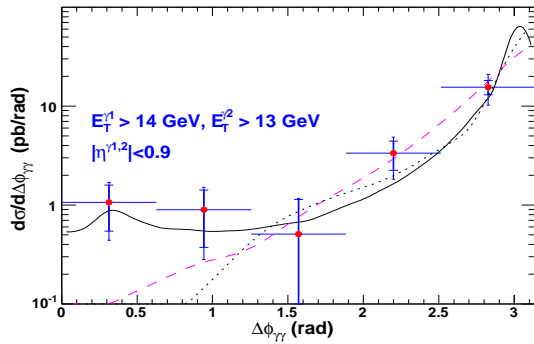calculation will be necessary.

FIG. 3: The $\Delta\phi$ angle between the two photons from the CDF Run II data, along with predictions from DIPHOX (solid), ResBos (dashed), and PYTHIA (dotted). The PYTHIA predictions have been scaled by a factor of 2. The bump at $\Delta\phi = 0.3$ on the DIPHOX curve is unphysical; it is caused by the combination of collinear divergence and the anti-collinear cut [11].

[1] ATLAS Collaboration, *Technical Proposal*, LHCC/P2 (1994); ATLAS Collaboration, *Physics Technical Design Report*, LHCC/99-15.

[2] CMS Collaboration, *Technical Proposal*, LHCC/P1 (1994).

[3] B. Abbott *et al.*, Phys. Rev. Lett. **86**, 1156 (2001).

[4] See, for example, G. F. Giudice and R. Rattazzi, Phys. Rep. **322**, 41 (1999) and references therein.

[5] T. Binoth, J. Ph. Guillet, E. Pilon and M. Werlen, Eur. Phys. J. C **16**, 311 (2000).

[6] C. Balazs, E. L. Berger, S. Mrenna and C.-P. Yuan. Phys. Rev. D **57**, 6934 (1998).

[7] T. Sjostrand, P. Eden, C. Friberg, L. Lonnblad, G. Miu, S. Mrenna and E. Norrbin, Computer Physics Commun. **135** (2001) 238. The PYTHIA version used in this analysis is 6.216.

[8] Z. Bern, L. J. Dixon and C. Schmidt, Nucl. Phys. Proc. Suppl. **116**, 178 (2003). [arXiv:hep-ph/0211216].

[9] In the CDF coordinate system, θ and ϕ are the polar and azimuthal angles, respectively, defined with respect to the proton beam direction, z. The pseudorapidity η is defined as $-\ln(\tan(\theta/2))$. The transverse energy of a particle is $E_T = E\sin(\theta)$.

[10] *The CDF II Detector Technical Design Report*, CDF collaboration, R. Blair et al., FERMILAB-Pub-96/390-E

[11] Y. Liu, FERMILAB-THESIS-2004-37.

[12] The photon isolation requirement efficiency is slightly E_T-dependent : 85% at 25 GeV, 78% at 60 GeV. Events in which a higher E_T photon is produced also tend to create a greater amount of ambient energy in the calorimeter, due to the effects of initial state soft gluon radiation.

[13] F. Abe *et al.* Phys. Rev. D **48**, 2998 (1993).

[14] D. Acosta *et al.*, Phys. Rev. D **65**, 112003 (2002) [arXiv:hep-ex/0201004].

[15] F. Abe *et al.*, Phys. Rev. Lett. **70**, 2232 (1993).

[16] Cross section tables for the different diphoton observables can be found at the HEPDATA database, durpdg.dur.ac.uk/HEPDATA/; see also [arXiv:hep-ex/0412050].

[17] S. Klimenko, J. Konigsberg and T. M. Liss, Fermilab-FN-0741 (unpublished).

[18] In addition, a double logarithmic divergence is present when the $\gamma\gamma$ q_T is exactly equal to the maximum hadronic energy allowed in the isolation cone. This is an example of what is known as a Sudakov shoulder. Since the logarithmic singularity is integrable over the bin size, no divergence is actually produced, but the calculational instability remains. The divergence is not present in the ResBos prediction, since it only appears at NLO in the fragmentation contribution. In the DIPHOX calculation, we have required less than 4 GeV of additional energy in the isolation cone, compared to the 1 GeV used in the experimental analysis. This looser theoretical isolation requirement improves the stability of the theory without having a significant impact on the numerical prediction.

[19] T. Binoth, J. Ph. Guillet, E. Pilon and M. Werlen, Phys. Rev. D **63**, 114016 (2003).